UDK 669.1:621.771.8
Original scientific article/Izvirni znanstveni članek

ISSN 1580-2949
MTAEC9, 58(3)349(2024)

FABRICATION AND PROPERTIES OF HIGH-CHROMIUM CAST IRON DISPERSED STEEL MATRIX COMPOSITE

IZDELAVA IN LASTNOSTI LITINE Z VISOKO VSEBNOSTJO KROMA DISPERGIRANE V JEKLENI KOMPOZITNI MATRICI

Guofeng Yuan*, He Wang, Xiuli Guo, Fei Zhao, Chengqi Yan, Han He

School of Mechanical Engineering, Anyang Institute of Technology, Anyang 455000, China

Prejem rokopisa – received: 2024-02-17; sprejem za objavo – accepted for publication: 2024-04-10

doi:10.17222/mit.2024.1111

Composites with high-chromium cast iron (HCCI) dispersed in a steel matrix were prepared using the multilayer rolling-forming method. The macroscopic morphology, microstructure and tensile properties of the bimetal composites were analyzed. The experimental results showed that brittle HCCI layers were necked and broken into uneven blocks or granules after hot-rolling forming. The fractured HCCI was encased in carbon steel completely, and the two metals achieved good metallurgical bonding. The Fe, Cr, Mn and C elements were diffused at the interface. The tensile strength of the composite was better than that of the as-cast iron. During the process of tensile deformation, the composite displayed a complex crack propagation rather than a fracture caused directly by brittleness. The damage tolerance and energy absorption capacity of the bimetallic composite were improved with a decentralized structure.

Keywords: hot rolling, high-chromium cast iron, dispersed, microstructure

Avtorji v članku opisujejo pripravo in karakterizacijo kompozitov jeklene litine z visoko vsebnostjo kroma (HCCI), ki je enakomerno porazdeljena (dispergirana) v jekleni matrici z nizko vsebnostjo ogljika (LCS; low carbon steel). Materiale so pripravili s postopkom oblikovanja z večplastnim valjanjem. Sledila je makroskopska analiza morfologije, mikrostrukture in nateznih lastnosti bimetalnih kompozitov. Eksperimentalni rezultati so pokazali, da so bile po vročem valjanju krhke HCCI plastistanjšane in nalomljene znotraj neravnih blokov ali granul. Prelom HCCI je bilpopolnoma obdan z LCS in obe kovini sta se med seboj dobro metalurško povezali. Elementi Fe, Cr, Mn in C so medsebojno difundirali na meji obeh kovin. Natezna trdnost kompozita je bila boljša od natezne trdnosti jeklene litine. Med procesom natezne deformacije kompozita je prednostno prišlo do kompleksnega procesa napredovanja razpok in manj kot posledica krhkega loma. Avtorji v zaključkih ugotavljajo, da sta bili odpornost na poškodbe in kapaciteta absorpcijske energije bimetalnega kompozita izboljšani zaradi decentralizacije strukture.

Ključne besede: vroče valjanje; jeklena litina z visoko vsebnostjo kroma;dispergiranost; mikrostruktura

1 INTRODUCTION

Wear-resistant materials have broad application prospects in modern engineering fields, such as mining, metallurgy, coal and transportation. Wear resistant parts often require good wear resistance and impact toughness during service.[1–3] High-chromium cast iron (HCCI), as a widely used wear-resistant material, has high hardness and excellent wear resistance. However, because of its poor impact toughness, HCCI fractures easily under impact fracture in engineering applications.[4–6]

In order to improve the comprehensive mechanical properties of HCCI, scholars often use the methods of micro-alloying, semi-solid forming, electric-pulse treatment, thermoplastic deformation and heat treatment to improve or refine the carbide in HCCI.[7–10] In addition, research on wear-resistant composite materials has been carried out. Composite materials of solid HCCI and ductile low-carbon steel (LCS) have good resistance to impact and wear as they effectively combine the advantages of the two metals, having an important application value in engineering.

At present, scientists often use duo-casting, surface compounding, diffusion bonding, casting and hot rolling to prepare HCCI/LCS bimetallic composites. Javaheri et al. prepared carbon steel and HCCI bimetallic composite materials with the liquid-solid casting bonding method.[11] They found that the elongation and impact toughness of the bimetal were lower than those of LCS and better than those of a single HCCI plate. Jilleh et al. studied the microstructure evolution of an HCCI surface welding layer, in which Nb and Mo were used as the main additives, while W and V were used as the secondary additives during the solidification process. The results showed that adding alloying elements helped refine the M_7C_3 carbide in HCCI.[12] Eroglu and Kurt successfully prepared HCCI/LCS composite materials through the hot pressure diffusion method. It was found that under a certain pressure (8 MPa), the bonding strength of the interface between the two metals was improved by increasing the diffusion temperature or time.[13] Xie et al. produced a sandwich-structured LCS/HCCI/LCS composite slab by casting, which was then subjected to multi-pass hot-roll-

*Corresponding author's e-mail:
aygxyygf@163.com (Guofeng Yuan)

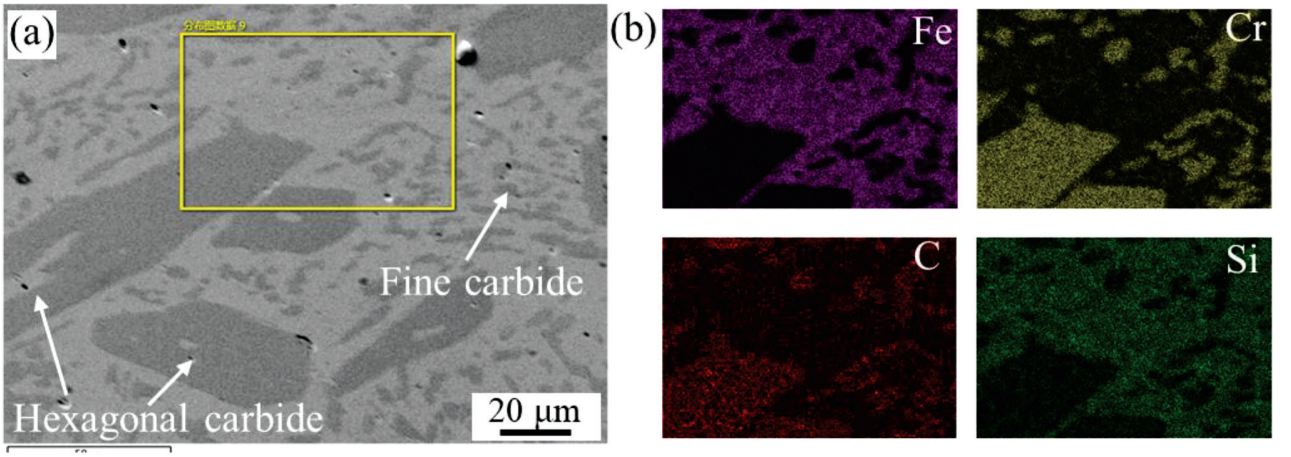

Figure 1: Microstructure of the as-cast HCCI: (a) SEM image and (b) results of the EDS analysis

ing deformation. They analyzed the microstructure of the interface between the two metals and discussed the influence of different heat-treatment processes on the microstructure.[14,15] In recent years, accumulative roll-bonding (ARB) technology, or multilayer rolling technology, has been favored by many scientists in the preparation of layered composites.[16–18] In the rolling forming process of bimetal multilayers, the two metals undergo plastic deformation together, finally producing a layered composite with a multilayer structure. However, if the mechanical properties of the two metals are different or the cumulative deformation is large, the harder layer will be necked and fractured with an increase in the strain or stress, forming granules or sheets which will be dispersed in the softer layer. At present, there are few studies on the preparation of HCCI/LCS composites with multilayer or cumulative rolling.

On the basis of the previous research, HCCI-dispersed composites were prepared by hot-rolling forming in this study. The macrostructure, microstructure and tensile properties of the composites were analyzed. The results provide a foundation and reference for the study of HCCI/LCS composites.

2 MATERIALS AND METHODS

2.1 Materials

As-received materials used in this study were 2.5 mm-thick as-cast HCCI sheets and 1 mm-, 2 mm- and 3 mm-thick commercial LCS sheets. Both HCCI and LCS sheets were cut into samples of (150 × 100) mm. The chemical compositions of HCCI and LCS are provided in **Table 1**.

Table 1: Chemical compositions (*w*/%) of HCCI and LCS

Material	C	Si	Cr	Mn	P	S	Mo	Ni	Fe
HCCI	2.8	1.1	28	1.0	0.02	0.02	0.5	0.4	balance
LCS	0.12	0.2	0.1	0.5	0.01	0.002	/	/	balance

Figure 1 shows a scanning electron microscope (SEM) microgram of the as-cast iron. A high volume fraction of hard $(Fe,Cr)_7C_3$ carbides was distributed in the matrix of HCCI, contributing to excellent wear resistance while greatly reducing the workability of HCCI.

2.2 Hot-rolling forming

In the present study, three kinds of slabs with different volume ratios were prepared, labeled as 1#, 2# and 3#. **Figure 2** illustrates the experimental process. For slab 1#, the thicknesses of HCCI and LCS were 2.5 mm and 1 mm, respectively, and the total number of the slab

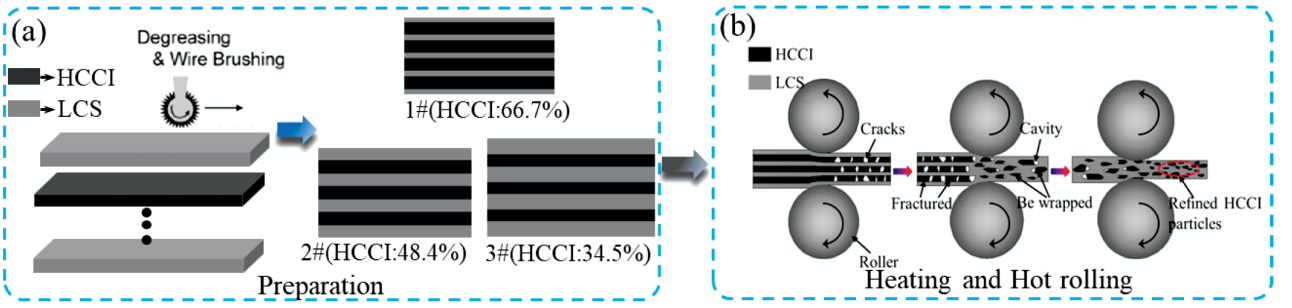

Figure 2: Schematic diagram of the experiment process: a) surface treatment and assembling and b) heating and hot-rolling forming

was nine. For slab 2#, the thicknesses of HCCI and LCS were 2.5 mm and 2 mm, respectively, and the total number of the slab was seven. For slab 3#, the thicknesses of HCCI and LCS were 2.5 mm and 3 mm, respectively, and the total number of the slab was seven. The LCS and HCCI sheets were stacked in an alternating sequence.

As shown in **Figure 2a**, the volume ratio of HCCI in the three types of slabs assembled was about 66.7, 48.4 and 38.5 %, respectively. The surface of the sheets was polished mechanically and cleaned with anhydrous ethanol. The composite slabs were sealed by argon arc welding and then pumped by a vacuum diffusion pump to a vacuum degree lower than 1×10^{-3} Pa. The prepared slabs were heated in a resistance furnace, and kept at the set temperature for 30 min before hot-rolling forming. During the process of hot-rolling deformation, the HCCI sheets with poor deformation performance would crack and fracture. Thus, a composite with HCCI dispersed in the steel matrix was prepared (**Figure 2b**). The composite slabs were hot-rolled at 1100 °C with a rolling rate of 0.2 m s^{-1}. The pass reduction was not more than 20 %. In the forming process, multi-pass (8-9 passes) reciprocating rolling was adopted. The cumulative rolling reductions of slabs 1#, 2# and 3# were (70, 75 and 77) %, respectively. The composite slabs were cooled in air after hot rolling. Hot-rolled slabs 1#, 2# and 3# were named CP1, CP2 and CP3, respectively.

2.3 Microstructure analysis

Specimens used for the microstructure analysis were cut from the RD-ND section. The metallographic specimens were mechanically polished and etched with a 4 % nitric acid-ethanol solution. Microstructure observation was carried out via an optical microscope (OM, Keyence VHX-2000) and a scanning electron microscope (SEM, SIGMA ZEISS) equipped with an energy dispersive spectroscope (EDS).

2.4 Property tests

Specimens used for the tensile test were cut from the middle of the sheets. The surfaces of the tensile specimens were mechanically polished to remove the surface oxide. The test specimens were processed to obtain the size specified in GB/T228.1-2010. The tensile deformation of the specimens verified the rolling direction. Tensile tests were carried out at room temperature using an AG-100 KN tensile test machine at a speed of 1 mm/min. The digital image correlation (DIC) technique was used to measure the localized tensile strain of the specimens. The tensile strain was analyzed based on the change in the position of black speckles scattered randomly on the surface of the specimen coated with white paint.[19,20] The fracture characteristics of the tensile specimens were observed and analyzed using the OM and SEM.

3 RESULTS AND DISCUSSION

3.1 Macrostructure of the composite

In order to show directly the distribution structure and shape of the two metals, the observation samples were cut by wire cutting from the middle of the rolled composite slab along the rolling direction. The sections were ground, polished and etched to better distinguish the two metals. **Figure 3** shows the macroscopic morphology of the RD-ND cross-sections of composites CP1 and CP3. As shown in the figure, the initial continuous layered structure of LCS and HCCI was no longer visible. Under the influence of large cumulative deformation, the HCCI layers with poor plastic deformation ability were necked and broken into uneven blocks or granules during rolling deformation. The fractured HCCI was completely encased in LCS.

In composite CP1, there was a relatively high volume of HCCI (about 66.7 %) during the forming process. After hot-rolling forming, LCS formed a continuous "mesh" structure, wrapping the broken HCCI. A "soft and hard" layer net coupling structure was generated. In this case, LCS with excellent plastic toughness can be seen as a toughness-enhancement phase embedded in brittle HCCI. Composite CP3 contained a relatively low volume of HCCI (about 38.5 %) during the forming process. After hot-rolling forming, HCCI was distributed in LCS as granules or sheets, forming a particle-dispersed structure. In this case, HCCI with a higher hardness can be considered as a particle-reinforced phase embedded in LCS.

Figure 4 displays macroscopic photographs of different cross-sections of the composite materials. The RD-TD cross-section of composite CP1 was revealed by removing a 0.3 mm-thick surface layer using a grinding machine. The RD-TD cross-sections of composites CP2 and CP3 were exposed after removing a 1.5 mm-thick surface layer. This treatment was mainly aimed to remove the oxide sheet formed during hot rolling and the thin LCS layer from the top layer. Due to its small vol-

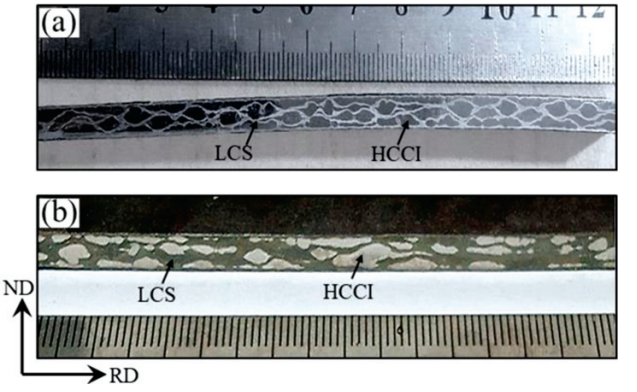

Figure 3: Macroscopic morphology of the composite: a) morphology of sample CP1 in the RD-ND section and b) morphology of sample CP3 in the RD-ND section

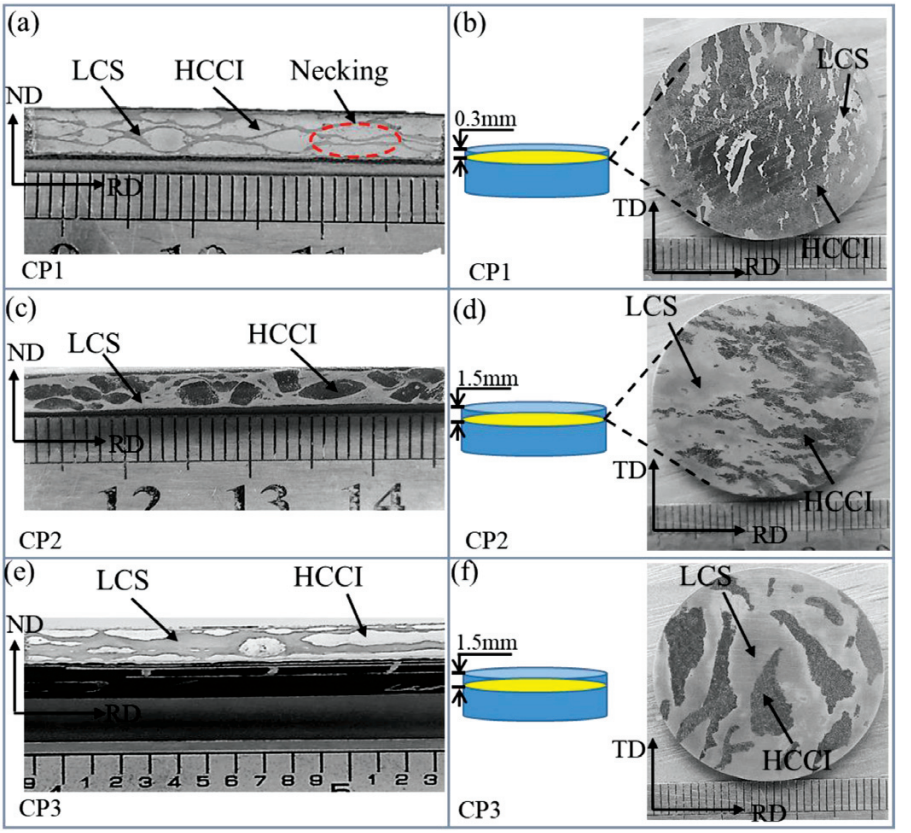

Figure 4: Macroscopic photographs of different cross-sections of the composite materials: a), b) sample CP1; c), d) sample CP2; and e), f) sample CP3

ume in the forming process, LCS from the RD-TD section of composite CP1 was distributed in HCCI as irregular spots or sheets. Similarly, in the RD-TD cross-section of composite CP3 containing a small volume of HCCI, HCCI was distributed in LCS as irregular sheets.

3.2 Microstructure of the composite

Figure 5 shows OM and SEM microstructure images of the RD-ND cross-sections of the three types of composites. Due to a serious shear deformation near the interface during the forming process, the joint interface between the two metals was irregularly wavy. The necked and fractured HCCI was wrapped by LCS. As shown in **Figure 5**, some parts of the adjacent LCS layers were bonded together. The two metal materials were well bonded, with no delamination or large crack observed at the bonding interface. After hot-rolling deformation, carbides in HCCI fractured and dissolved (**Figure 5f**). Meanwhile, defects such as partial micro-cracks and carbide micro-holes that were not filled by the matrix were detected in fractured carbides (indicated by red circles in **Figures 5f** and **6a**).

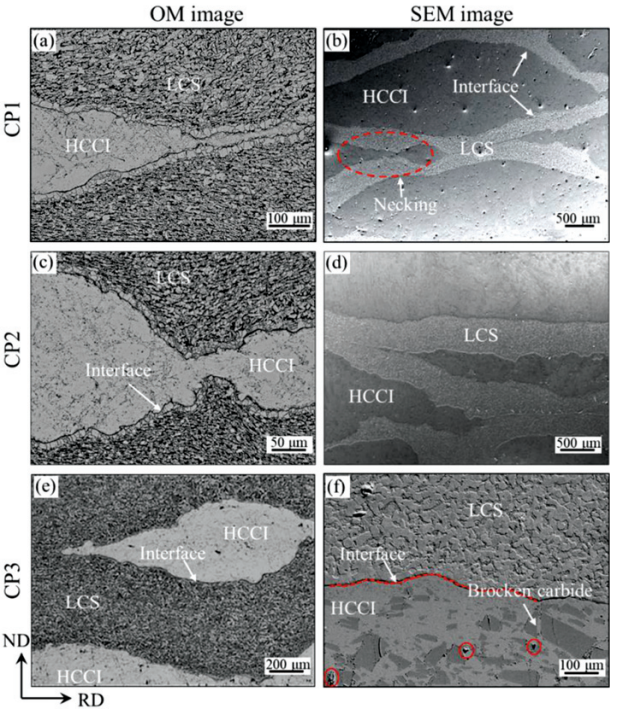

Figure 5: Microstructures of three composites: a), b) sample CP1, c), d) sample CP2, and e), f) sample CP3

Figure 6 shows a microstructure image of the bonding interface and EDS analysis results for composite CP3. The interface of the two metals was curved and undulating. A carbon-poor ferrite band was formed near the steel side at the interface (**Figure 6a**). Different contents of the elements in the two metals led to a concentration

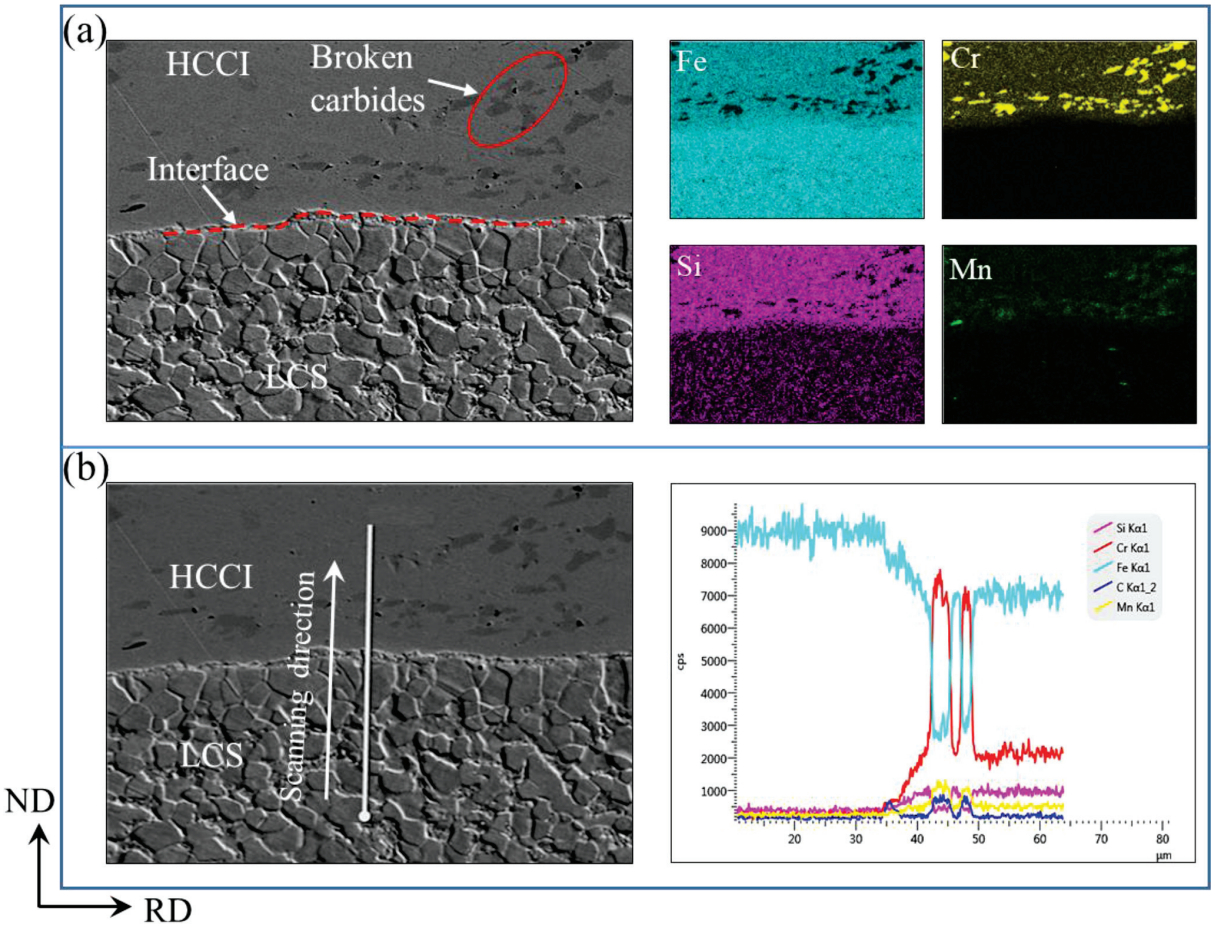

Figure 6: EDS analysis of the bonding interface of sample CP3: a) SEM image, b) distribution of elements, c) and d) line analysis

difference at the interface. Fe, Cr, Mn and Si were diffused at the interface between the two metals. Cr, Si and Mn moved from HCCI to LCS, and Fe migrated from LCS to HCCI. The C element was mainly distributed at the bonding interface and in the carbides of HCCI. According to the line scanning analysis, the contents of Fe, Cr, Mn and Si formed a step-like gradient distribution at the interface, and the diffusion distance of the elements at the interface was about 4–8 μm. A continuous diffusion of the elements at the bonding interface indicated a successful generation of a metallurgical bond.[21]

3.3 Mechanical properties

The tensile properties and fracture characteristics of the composites were analyzed. **Figure 7** depicts the engineering stress-strain curves of the as-cast HCCI and composite materials. HCCI fractured directly due to brittleness during the tensile process, and its elongation was low. The overall tensile strength and elongation of the composites were better than those of the as-cast HCCI. The average tensile strength of composites CP1, CP2 and CP3 was 148.2, 203.1 MPa and 223.7 MPa, respectively. Compared with HCCI, the composites prepared had better tensile properties, which is attributed to the addition of LCS with good strength and plasticity. The tensile strength and elongation of the composites gradually increased with the increase in the volume ratio of LCS. In addition, it can be seen from **Figure 7** that when the stress reached the maximum, the stress-strain curve of

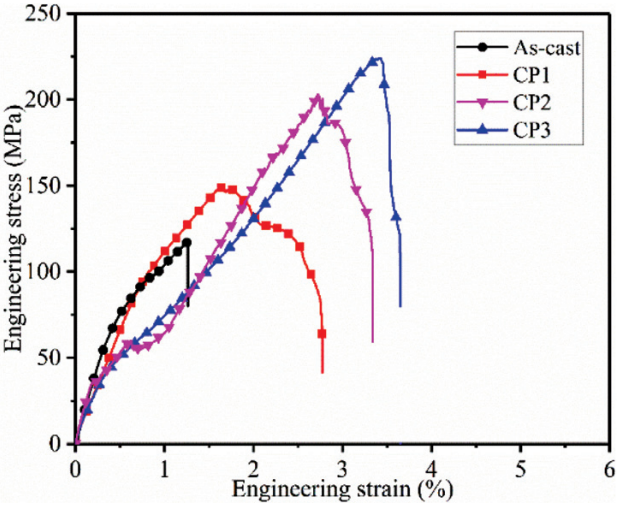

Figure 7: Engineering stress-strain curves of the as-cast HCCI and composite materials

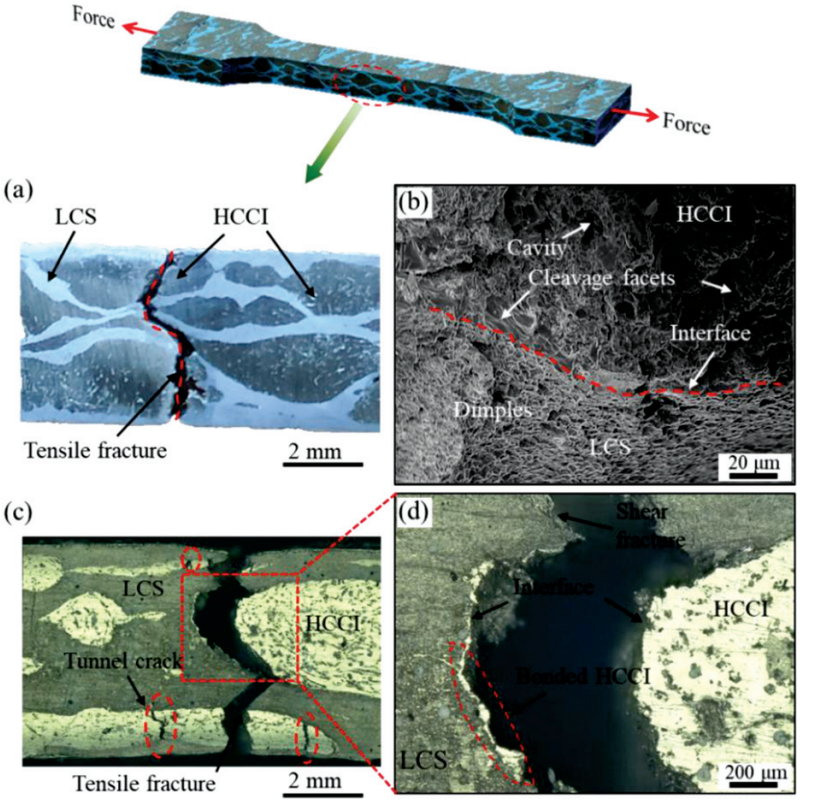

Figure 8: Fracture characteristics of the composite materials: a), b) CP1, c), d) CP3

the composite materials did not terminate in a brittle fracture, but entered a fluctuation stage.

Figure 8 describes the fracture characteristics of tensile specimens CP1 and CP3. The fracture morphology presents a curved and complex expansion process without an obvious stratification. Figure 8b shows the microstructure of fractured composite CP1. It is evident that the two metals were closely bonded, with no crack observed at the interface. The fracture morphology of the LCS side is mainly dimple-shaped, indicating its good plastic-deformation ability. There are many cleavage planes and micro-pores formed due to carbide stripping in the fractured HCCI, showing typical brittle fracture characteristics.

Figure 9 displays the strain distribution along the RD direction of composite CP3 measured with DIC at different tensile stages. Due to the difference in the properties of the two metals, the surface of the composite underwent uneven deformation during the initial elastic-deformation stage. With an increase in the deformation amount, more yellow spots with a large local strain were formed on the specimen surface (indicated by red triangular arrows in **Figure 9**). These spots might have been the source of cracks in brittle HCCI during the deformation process. During deformation, the material did not fracture directly due to brittleness, but experienced a complex process where multiple cracks were formed and expanded. As the deformation progressed, one of the

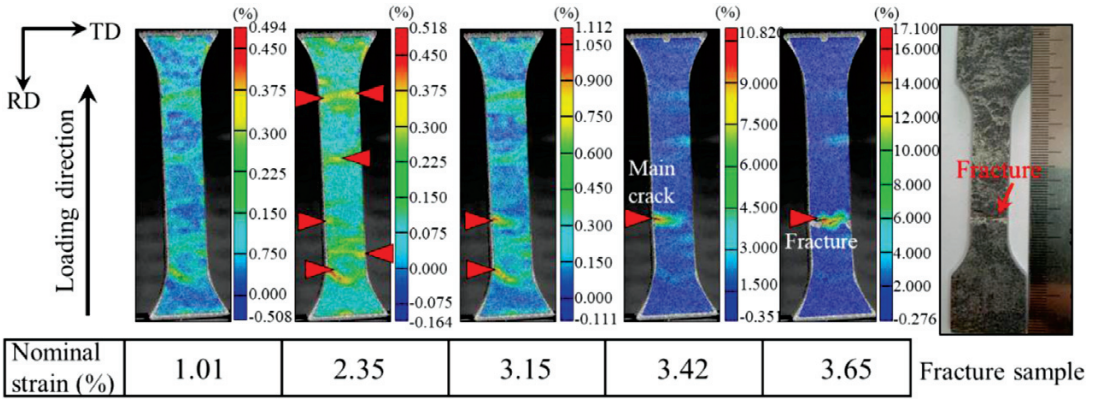

Figure 9: Strain distribution along the RD direction of sample CP3 at different tensile strain stages

cracks might have become the main crack and expanded rapidly until the specimen finally broke. Different from brittle HCCI, the bimetallic composite had a unique three-dimensional distribution structure, which effectively improved the damage tolerance and energy absorption of the composite.

4 CONCLUSIONS

In this paper, composites with HCCI distributed in the steel matrix were prepared using the hot-rolling forming method. The macroscopic morphology, microstructure and mechanical properties of the composites were analyzed. The following conclusions are drawn:

(1) The composites with HCCI distributed in the steel matrix were successfully prepared by hot-rolling bonding. The HCCI layers with poor plastic-deformation performance were necked and broken into uneven blocks or granules after hot-rolling forming. The fractured HCCI was completely encased in LCS.

(2) After hot-rolling forming, a good metallurgical bond was formed between the two metals. The Fe, Cr, Mn and C elements were diffused along the interface.

(3) The tensile strength of the composites was better than that of the as-cast iron. The average tensile strength of composites CP1, CP2 and CP3 was 148.2, 203.1 and 223.7 MPa, respectively.

(4) The tensile fracture morphology of the composites showed a complex expansion process, and multiple tunnel cracks were formed in brittle HCCI. The damage tolerance and energy absorption capacity of bimetallic composites were improved with the dispersion of HCCI in the steel matrix.

Acknowledgments

This work was funded by the Doctoral Research Start-Up Fund of the Anyang Institute of Technology (No. BSJ2023003), the Henan Science and Technology Plan Project (No. 232102230060) and the Key scientific research projects of colleges and universities of the Henan Province (No. 24B430003).

5 REFERENCES

[1] F. G. Lu, S. Z. Wei, L. J. Xu, Y. C. Zhou, X. D. Wang, F. F. Wang, X. Y. Yi, Erosion-Wear Behaviors of High-Chromium Cast Iron with High Nitrogen Content in Water-Sand Slurry and Acid-Sand Slurry, Tribol. Trans., 63 (**2020**), 325–335, doi:10.1080/10402004.2019.1690082

[2] Y. C. Li, P. Li, K. Wang, H. Z. Li, M. Y. Gong, W. P. Tong, Microstructure and Mechanical Properties of a Mo Alloyed High Chromium Cast Iron after Different Heat Treatments, Vacuum, 156 (**2018**), 59–67, doi:10.1016/j.vacuum.2018.07.013

[3] J. Cui, L. Guo, H. Lu, D. Y. Li, Understanding Effects of Cr Content on the Slurry Erosion Behavior of High-Cr Cast Irons Through Local Property Mapping and Computational Analysis, Wear, 376 (**2017**), 587–594, doi:10.1016/j.wear.2016.12.031

[4] Z. Y. Chen, H. G. Fu, F. Wang, N. B. Yuan, J. Lin, Effect of Si on Microstructure and Wear Resistance of Hypereutectic High-Chromium Cast Iron, J. Mater. Eng. Perform., 32 (**2022**), 5450–5465, doi:10.1007/s11665-022-07475-z

[5] C. Vergne, C. Boher, R. Gras, C. Levaillant, Influence of oxides on friction in hot rolling: experimental investigations and tribological modelling, Wear, 92 (**2006**), 957–975, doi:10.1016/j.wear.2005.06.005

[6] F. J. Belzunce, A. Ziadi, C. Rodriguez, Structural integrity of hot strip mill rolling rolls, Eng. Fail. Anal., 11 (**2004**), 789–797, doi:10.1016/j.engfailanal.2003.10.004

[7] E. Waleed, R. Rashad, E. Sayed, E. Saied, Influence of Vanadium and Boron Additions on the Microstructure, Fracture Toughness, and Abrasion Resistance of Martensite-Carbide Composite Cast Steel, Adv. Mater. Sci. Eng., 7 (**2016**), 1–8, doi:10.1155/2016/1203756

[8] B. Y. Geng, R. F. Zhou, Y. K. Li, Q. P. Wang, Y. H. Jiang, The difference in effects of electric current pulses on inoculation of austenite and M_7C_3 carbides, Mater. Res. Express, 7 (**2020**), doi:10.1088/2053-1591/abb2d0

[9] X. H. Zhi, J. D. Xing, H. G. Fu, B. Xiao, Effect of niobium on the as-cast microstructure of hypereutectic high chromium cast iron, Mater. Lett., 62 (**2008**), 857–860, doi:10.1016/j.matlet.2007.06.084

[10] Y. Pei, R. B. Song, Y. C. Zhang, L. Huang, C. H. Cai, E. Wen, Z. Y. Zhao, P. Yu, S. Y. Quan, S. R. Su, C. Chen, The relationship between fracture mechanism and substructures of primary M_7C_3 under the hot compression process of self-healing hypereutectic high chromium cast iron, Mat. Sci. Eng. A., 779 (**2020**), 139150, doi:10.1016/j.msea.2020.139150

[11] V. Javaheri, H. Rastegari, M. Naseri, Fabrication of plain carbon steel/high chromium white cast iron bimetal by a liquid–solid composite casting process, Int. J. Min. Met. Mat., 22 (**2015**), 950–955, doi:10.1007/s12613-015-1154-3

[12] A. Jilleh, N. K. Babu, V. Thota, A. L. Anis, M. K. Harun, M. K. Talari, Microstructural and wear investigation of high chromium white cast iron hardfacing alloys deposited on carbon steel, J. Alloy. Compd., 857 (**2020**), 157472, doi:10.1016/j.jallcom.2020.157472

[13] M. Eroglu, B. Kurt, Diffusion bonding between high chromium white iron and low carbon steel, Mater. Sci. Tech., 23 (**2007**), 171–176, doi:10.1179/174328407X154202

[14] G. L. Xie, H. Sheng, J. T. Han, J. Liu, Fabrication of high chromium cast iron/low carbon steel composite material by cast and hot rolling process, Mater. Design, 31 (**2010**), 3062–3066, doi:10.1016/j.matdes.2010.01.014

[15] G. L. Xie, J. T. Han, J. Liu, Z. Y. Jiang, Texture, microstructure and microhardness evolution of a hot-rolled high chromium cast iron, Mat. Sci. Eng. A., 527 (**2010**), 6251–6254, doi:10.1016/j.msea.2010.06.036

[16] R. Cao, Y. Ding, Y. J. Yan, X. B. Zhang, J. H. Chen, Effect of heat treatment on interface behavior of martensite/austenite multilayered composites by accumulative hot roll bonding, Compos. Interface, 26 (**2019**), 1069–1085, doi:10.1080/09276440.2019.1583007

[17] M. Huang, C. Xu, G. Fan, E. Maawad, W. M. Gan, L. Geng, F. X. Lin, G. Z. Tang, H. Wu, Y. Du, D. Y. Li, K. Miao, T. T. Zhang, X. S. Yang, Y. P. Xia, G. J. Cao, H. J. Kang, T. M. Wang, T. Q. Xia, H. L. Xie, Role of layered structure in ductility improvement of layered Ti/Al metal composite, Acta. Mater., 153 (**2018**), 235–249, doi:10.1016/j.actamat.2018.05.005

[18] M. Azimi, M. R. Toroghinejad, M. Shamanian, L. A. I. Kestens, Grain and texture evolution in nano/ultrafine-grained bimetallic Al/Ni composite during accumulative roll bonding, J. Mater. Sci., 53 (**2018**), 12553–12569, doi:10.1007/s10853-018-2510-2

[19] J. Park, M. C. Jo, T. Song, H. S. Kim, S. S. Sohn, S. Lee, Ultra-high strength and excellent ductility in multi-layer steel sheet of austenitic hadfield and martensitic hot-press-forming steels, Mat. Sci. Eng. A., 759 (**2019**), 320–328, doi:10.1016/j.msea.2019.05.046

[20] M. S. Kim, K. S. Park, D. I. Kim, J. Y. Suh, J. H. Shim, K. T. Hong, S. H. Choi, Heterogeneities in the microstructure and mechanical

properties of high-Cr martensitic stainless steel produced by repetitive hot roll bonding, Mat. Sci. Eng. A., 801 (**2021**), 140416, doi:10.1016/j.msea.2020.140416

[21] X. Li, Y. H. Sun, Z. Q. Wang, F. C. Jiang, Fabrication, microstructure characterization and mechanical property of the Ti6Al4V-(NiTif/Mg3AlZn) laminate composite, J. Alloys Compd., 774 (**2019**), 656–667, doi:10.1016/j.jallcom.2018.10.074

[22] B. X. Liu, L. J. Huang, B. Kaveendran, L. Geng, X. P. Cui, S. L. Wei, F. X. Yin, Tensile and bending behaviors and characteristics of laminated Ti-(TiBw/Ti) composites with different interface status, Compos. Part B: Eng., 108 (**2017**), 377–385, doi:10.1016/j.compositesb.2016.10.001